Optical Feedback FM-to-AM Conversion With Photonic Integrated Circuits for Displacement Sensing Applications

Clément Deleau, Han Cheng Seat, Frederic Surre, Usman Zabit, Francis Jayat, Thierry Bosch, Olivier Bernal

Optical Feedback FM-to-AM Conversion with Photonic Integrated Circuits for Displacement Sensing Applications

Clément Deleau[1], Han Cheng Seat[1], Frederic Surre[2], Usman Zabit[3]
Francis Jayat[1], Thierry Bosch[1], Olivier Bernal[1]
[1]LAAS-CNRS, University of Toulouse, CNRS, INP, Toulouse, FRANCE
[2]James Watt School of Engineering, University of Glasgow, Glasgow, UK
[3]National University of Sciences and Technology (NUST), Islamabad, PAKISTAN
DOI:10.1109/JLT.2024.3355048

***Abstract*—In this paper, integrated silicon nitride edge filters are demonstrated to perform the function of frequency to amplitude (FM-to-AM) conversion of optical feedback interferometric (OFI) signals. Compared to existing OFI FM-to-AM conversion techniques employing optical edge filters based on gas cells, and free-space or fiber-based Mach Zehnder interferometers (MZIs), integrated photonic processing of OFI signals is found to offer greater compactness and design flexibility. In addition, higher resilience to parasitic mechanical vibrations and better temperature control of the photonic chip can potentially facilitate sensing system operation. Three different optical filters have been implemented to perform FM-to-AM conversion: two integrated MZIs with a 2- cm and 4- cm path-length imbalance, respectively, and one micro-ring resonator (MRR). The OFI FM-to-AM conversion factors are experimentally determined to be 0.37 GHz^{-1}, 0.65 GHz^{-1} and, 1 GHz^{-1} for the 2- cm imbalanced MZI, the 4- cm imbalanced MZI and the MRR, respectively. The corresponding noise equivalent displacements (NEDs) with optical chip coupling are found to be approximately 25.4 nm, 11.5 nm and 4.9 nm, respectively, over a 1 kHz bandwidth. The results are compared to those obtained with a reference hydrogen cyanide gas cell exhibiting a sensitivity of approximately 0.25 GHz^{-1} and an NED of 5.6 nm.**

***Keywords*—Integrated Photonics, Self-Mixing, Optical Feedback Interferometry, Laser Sensors, Silicon Nitride, Mach Zehnder interferometer, Micro-Ring Resonator**

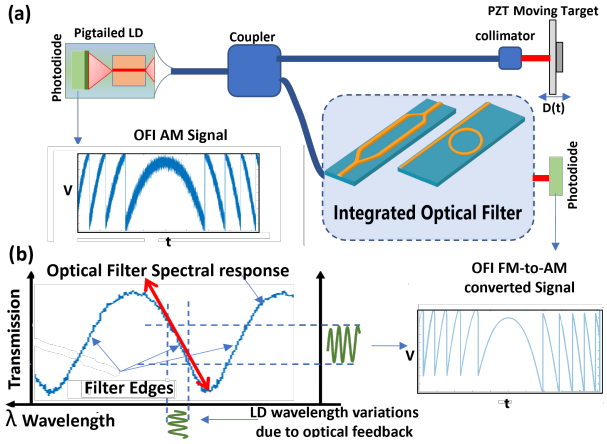

Fig. 1: (a) Proposed OFI sensing scheme using LD, a piezoelectric transducer (PZT) as a target, showing in particular the AM channel retrieved from a monitoring PD and light partially coupled in integrated optical filters for FM channel demodulation. (b) OFI frequency modulation signal (FM channel) embedded in the laser frequency is converted into amplitude modulation (AM) by using the fringe edge of an optical filter.

I. Introduction

Optical feedback interferometry (OFI), which is also referred to as the self-mixing (SM) effect in laser diodes (LDs), has gained widespread attention in recent years. This technique provides a self-aligned and cost-effective sensing system, and is frequently used for measuring displacement, vibration, and velocity, among many other parameters [1], [2]. To achieve the necessary performance in precision displacement reconstruction, numerous signal processing techniques have previously been devised [3]–[6].

In OFI, the backscattered laser beam from a target placed at a certain distance away re-enters the active LD cavity, thereby directly perturbing the cavity optical field. Consequently, modulations of both amplitude (AM) and frequency (FM) of the field can occur, as described by the Lang and Kobayashi equations [7]. Contrary to the FM channel, the OFI information embedded in the optical power modulation (or AM channel) is either directly available from the monitoring photodiode (PD) located behind the LD cavity or by monitoring a fraction of the optical power subsequently emitted by the LD. Nevertheless, the signal-to-noise ratio (SNR) of FM OFI signals is approximately two orders of magnitude better than its AM equivalent, as demonstrated in [8]. This suggests that FM OFI signals are potentially capable of enhancing the sensitivity of OFI, not just for low-noise small displacement applications, but also for non-cooperative diffusive remote target surfaces where the back-scattered OFI signal is generally weak in magnitude. FM channel signals are thus crucial for improving the effectiveness of OFI.

ANR-20-CE42-0010 PICSONDE

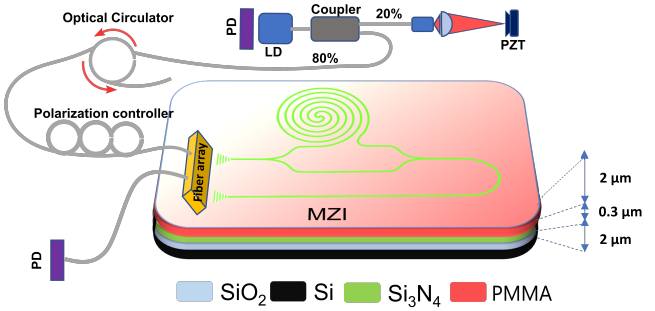

Fig. 2: Schematic diagram of one of the three OFI FM-to-AM systems comprising one LD, two PDs, one fiber array, an integrated MZI used as OFI FM-to-AM filter implemented in silicon nitride with a Poly(methyl methacrylate) (PMMA) polymer cladding layer and a PZT as remote target.

The principle of FM-to-AM conversion is illustrated in Fig.1 (b) where the modulated laser wavelength induced by OFI is converted into optical power modulation using one edge of an optical filter. In the work by Contreras *et al.* [9], an acetylene gas cell was employed as the OFI converting filter. By taking advantage of the steep edge of an optical absorption line of the gas cell, a typical OFI FM-to-AM conversion factor of approximately 2.2 GHz^{-1} was achieved with a typical absorption line depth of 8 dB. Other approaches for OFI FM-to-AM conversion have also been reported, such as using free-space and fiber-based Mach Zehnder interferometers (MZIs) [8], [10]. These approaches offer improved sensitivity and flexibility compared to gas cell-based filters. In particular, MZIs allow for easier tuning of the laser wavelength and adjustment of the sensitivity via optical path length imbalance of the two arms. In [8], a sensitivity of 19 $(\text{GHz})^{-1}$ was achieved, which is approximately 10 times better than the gas cell-based filter [9], with a noise equivalent displacement (NED) of 1.3 pm/$\sqrt{Hz}$. However, both approaches require cumbersome setups and are generally prone to temperature and mechanical perturbations.

Here, we propose and implement integrated optical interferometers [11] and resonators to perform the OFI FM-to-AM conversion, as illustrated in Fig.1. The devices are fabricated in silicon nitride, since Si_3N_4 has relatively low propagation loss and a lower thermo-optic coefficient ($\sim 2.45 \cdot 10^{-5}$RIU/K) compared to silicon photonics ($\sim 1.8 \cdot 10^{-4}$RIU/K) at 1550 nm [12]. We also demonstrate the possibility to fully integrate this conversion scheme on chip for more efficient tuning of the filter. This serves to further improve the sensor robustness against temperature variations and parasitic mechanical vibrations as compared to fiber-based implementation [8]. Two MZIs and a micro-ring resonator (MRR) are implemented to achieve different sensitivities. The results obtained are compared to those obtained using a reference Hydrogen Cyanide (HCN) gas cell from Wavelength References, Inc (HCN-13-H(16.5)-25).

An overview of the FM OFI signal is presented in Section II, followed by the description of our proposed integrated OFI FM-to-AM conversion approach. Section III next describes the photonic circuit design, while fabrication and experimental results are presented in Section IV. Section V discusses the performances achieved and proposes future improvements before concluding this paper.

II. Integrated OFI FM-to-AM Demodulation

A. Overview of FM OFI

In the more widely known AM channel, OFI induces fluctuations in the optical output power (OOP) of the LD that can be given by [1]:

$$P(t) = P_0 \left[1 + m_i \cos\left(\Phi_F(t)\right)\right], \tag{1}$$

where P_0 is the emitted optical power under free-running conditions, m_i the modulation index and $\Phi_F(t)$ the laser output phase in the presence of feedback. $\Phi_F(t)$ is related to the laser output phase without feedback $\Phi_0(t) = 4\pi D(t)/\lambda_0$, with $D(t)$ the laser-target distance, by [1], [2]:

$$\Phi_0(t) = \Phi_F(t) + C \sin\left(\Phi_F(t) + \arctan\alpha\right), \tag{2}$$

with α the linewidth enhancement factor of the laser and C the optical feedback factor. Depending on C, the laser can operate in different regimes. SM sensing is generally performed under either weak feedback regime ($C < 1$), moderate feedback regime ($1 < C < 4.6$), or strong feedback regime ($C > 4.6$). However, a moderate feedback regime is generally preferred as the apparently simple saw-tooth shaped SM fringes associated with this regime [13] intrinsically provide directional indication and require only simplified SM fringe detection processing [3].

In the case of OFI FM channel, eq. (2) can also be re-written as follows:

$$\left[\nu_0(t) - \nu_F(t)\right]\tau_{ext} = \frac{C}{2\pi}\sin\left(2\pi\nu_F(t)\,\tau_{ext} + \arctan\alpha\right), \tag{3}$$

where ν_0 is the unperturbed LD frequency, ν_F the LD frequency under optical feedback, and τ_{ext} the external round trip time of flight. From (3), the variation of the LD frequency $\Delta\nu = \nu_F - \nu_0$ is strongly constrained as

$$|\Delta\nu| \leq \frac{C}{2\pi\tau_{ext}}. \tag{4}$$

The design of the optical filter should thus consider this maximum span to avoid folding. Note that fringe-locking to the half fringe [8] can extend this range further and can thus potentially allow the design of an even steeper filter.

As previously mentioned, OFI FM-to-AM conversion can be performed using the edge of an optical filter, as illustrated in Fig. 1.Here, both integrated MZIs and MRRs are employed.

B. OFI FM-to-AM conversion by MZI

In the case of MZI being employed, the output power P_{out}^{MZI} can be expressed as

$$P_{out}^{MZI} = \frac{P_{in}}{2}\left[1 + \cos\left(2\pi n(\nu)\frac{\Delta d_{path}}{c}\nu\right)\right], \tag{5}$$

where P_{in} is the injected optical power in the MZI, Δd_{path} the MZI path length difference, n the effective index of the optical path and c the speed of light in vacuum. As reported in [8], the maximum sensitivity S_{MZI} is achieved at the middle of the transmission power response of the MZI. From (5), the MZI's periodic response can release the constraint on the positioning of the LD wavelength by adjusting the laser parameters (temperature, drive current), or by using electro-optic or thermo-optic effects on the MZI. S_{MZI} can thus be given as

$$S_{MZI} = \frac{1}{P_{in}} \frac{\partial P}{\partial \nu},\ S_{MZI_{max}} = \pi n_g(\lambda) \frac{\Delta d_{path}}{c}, \quad (6)$$

where λ is the LD wavelength in vaccuum and n_g the group index defined as $n_g(\lambda) = n(\lambda) - \lambda \frac{\partial n(\lambda)}{\partial \lambda}$. In the case of integrated MZIs, it is more convenient to express S as a function of the free spectral range FSR(λ), as defined below:

$$FSR(\lambda) = \frac{\lambda^2}{n_g(\lambda)\Delta d_{path}}. \quad (7)$$

Consequently, (6) can be re-written as

$$S_{MZI_{max}} = \pi \frac{\lambda^2}{c \times FSR}. \quad (8)$$

For the open-loop OFI approach, similar to bandwidth definition, it is useful to define the range $\delta\lambda_{dyn}$ for which the sensitivity is reduced by a factor of $\sqrt{2}$. It can be shown from (6) that $\delta\lambda_{dyn}$ can then be approximated by:

$$\delta\lambda_{dyn} \sim \frac{\lambda^2}{4n(\lambda)\Delta d_{path}}. \quad (9)$$

This conversion range should ideally cover not only the LD wavelength variation induced by OFI but also the wavelength variation induced by LD current modulation that might be required for dithering [14]. There is thus a trade-off between sensitivity and conversion range for open-loop configurations.

C. OFI FM-to-AM conversion by MRR

The resonant condition for a given mode number m in a circular MRR can be given by:

$$m\lambda_m = 2\pi r n_{eff}, \quad (10)$$

where r is the MRR radius, λ_m the wavelength of the m^{th} resonance, n_{eff} the effective index of the MRR optical path and m an integer.

In the case of symmetrical and lossless coupling to the MRR, the transmitted output power P_{out}^{MRR} can be represented by [15]:

$$P_{out}^{MRR}(\lambda) = P_{in}(\lambda)\left|\frac{\tau - \alpha_R e^{j\phi_R}}{1 - \tau\alpha_R e^{j\phi_R}}\right|^2, \text{ with } \phi_R = 2\pi L_R n_{eff}/\lambda \quad (11)$$

where P_{in} is the spectrally-dependent optical power that is injected into the MRR, λ the wavelength in vacuum, τ the self-coupling coefficient of the resonator's coupler, $L_R = 2\pi r$ the length of MRR, and α_R expresses the attenuation caused by light scattering and absorption during round trip field transmission. The phase shift experienced by the lightwave propagating through the ring over a single pass is denoted by ϕ_R. When the internal losses are equal to the cross-coupling, also known as critical coupling [15], a state of perfect destructive interference can be achieved. This results in maximum extinction ratios in the resonance spectrum. Under this condition, the cross-coupling coefficient can be represented by κ, satisfying the equality $\kappa^2 + \tau^2 = 1$. The Full-Width-Half-Maximum (FWHM) of the resonance can then be approximated by:

$$FWHM = \frac{\kappa^2 \lambda^2}{L_R n_g \pi} \quad (12)$$

Consequently, the sensitivity of the MRR is related to its quality factor Q and depth of modulation M, both of which will depend on the coupling, absorption and scattering properties of the MRR; while in the case of the MZI, its sensitivity is directly proportional to Δd_{path} and inversely proportional to the FSR. Now, since the MRR transmission characteristics are very similar to a Lorentzian shape, the MRR sensitivity can be approximated by:

$$S_{MRR_{max}} \sim \frac{\pi}{2} \frac{\lambda^2}{c \times\ FWHM} \quad (13)$$

The advantages of the MRR over the MZI are its significantly more compact footprint, thus suggesting easier implementation (since it is less cumbersome) and lower cost. The main drawback is that the MRR's FSR is generally much wider than that of the MZI for similar filter sensitivities, which might subsequently require more effort in adjusting the LD wavelength to match the edge of the optical filter.

III. Design and Fabrication

A. Waveguide design

As previously mentioned, it can be advantageous to reduce temperature effects on the filter response by design. These effects on the PIC can nonetheless be relaxed a second time at the system level by using a temperature controller, which can also be used to adjust the position of the optical filter on the spectrum. Therefore, by taking into account the low positive thermo-optic index of Si_3N_4 and the negative one of the typical polymer cladding, the waveguide width is designed to be 1.6 µm. This allows a low thermo-optical effective coefficient of the fundamental mode of -2.5·10^{-5} RIU/K to be obtained while also reducing field superposition at the potentially rough waveguide side-walls, which is one of the main sources of optical loss.

B. MZI and MRR design

For simplicity, the MZIs are implemented using two Y-splitters to ensure balanced partition of the optical power injected into the two arms. Two different imbalanced arms of 2-cm and 4-cm length are designed. The theoretical sensitivities that can be achieved are 0.42 GHz^{-1} and 0.84 GHz^{-1}, respectively, for the 2 imbalanced MZIs.

Fig. 3: Microscope image of the fabricated Si_3N_4 MRR.

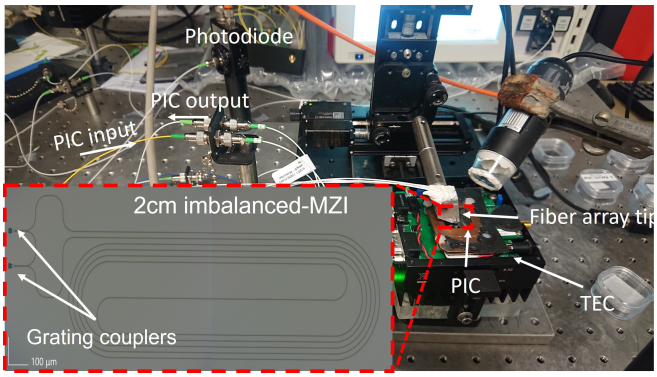

Fig. 4: Experimental setup with fiber array and integrated photonic chip positioned on top of thermo-electric cooler (TEC). Inset shows microscope photograph of 2 cm imbalanced MZIs.

In this work, the design of the MRR simply consists of coupling a straight waveguide to a circular ring resonator with radius r= 120 µm. The expected FSR_{MRR} is ∼ 1.6 nm which is approximately 12-25 times larger than that of the two MZIs.

C. Layout

Lightwave from LD is here transmitted by fiber arrays (Precision Micro Optics) to the grating couplers fully etched with a 30° incidence angle to be injected into the photonic circuits. These couplers facilitate the testing of different structures implemented on the same die [16]. While alignment is greatly simplified using grating couplers, the main drawback for our application is the higher injection loss compared to other techniques, such as edge coupling. Further, as only one-dimensional grating couplers are employed, only one single polarization can be injected into the photonic circuits (here TE polarization). Consequently, a polarization controller is used to further improve the injection efficiency. The performance of the grating couplers is characterized and de-embedded to facilitate the analysis of the proposed system.

D. Fabrication process

As illustrated in Fig. 2, the integrated photonic circuits are fabricated using a stoichiometric 300 nm thick Si_3N_4 or silicon nitride (SiN) on 2- µm silicon oxide on an Si wafer from Microchemicals. This wafer was fabricated using Low-Pressure Chemical Vapor material deposition to reduce hydrogen impurities that could lead to absorption losses. The index of the SiN as the core material is measured by ellipsometry to be n_{core} ∼ 1.97 at 1550 nm [12]. The bottom oxide here prevents optical leakage into the silicon during propagation. Electron-beam (E-beam) lithography from a RAITH150 E-beam writer is employed to pattern the waveguides, MZIs, MRR and grating couplers. Here, an electron-sensitive MaN2405 resin is deposited by spin coating, and is used together with an Electra92 resin layer desposited on top for electronic charge dissipation during the exposure process. The main E-beam exposure parameters, namely acceleration voltage, beam current, step size and dose, are respectively 20 kV, 37 pA, 10 nm and 112 µC/cm^2 for the MaN2405 resist. After the resist development, the SiN layer (∼ 300 nm thick) is etched using Reactive Ion Etching (RIE) to obtain all the photonic structures. The remaining MaN2405 resist is then removed using acetone solution followed by Plasma O_2 cleaning. Finally, a 2- µm PMMA resin is simply deposited on top as the cladding layer for waveguide protection.

IV. Experimental Results

A. Experimental setup

The experimental setup employed for characterizing the FM-to-AM conversion using these integrated optical filters is illustrated in Fig. 4, together with an inset showing a typical 2-cm imbalanced MZI. The light source used in this work is a fiber pigtailed WSLD-1550-020m LD from Wavespectrum emitting 8.6 mW of power at λ=1550 nm for a drive current of 45 mA. This emitted light is then injected into a 1 x 2 80/20 fiber coupler, as previously shown in Fig. 2. The output from the coupler is split into (1) the measurement arm which connects the LD to the target, and (2) the OFI FM-to-AM conversion photonic chip. The lead-in light from a fiber array with a 30° polished angle is injected into the photonic circuits via integrated grating couplers. In order to facilitate the testing process, the fiber array probes are not glued to the chip with epoxy. Hence, the lead-in fiber tips could potentially be prone to unwanted vibrations, thereby generating parasitic reflections. Subsequently, a fiber circulator is added to reduce or suppress any parasitic feedback from the FM-to-AM arm. For better interference stability, a polarization controller is also added to tune the polarization state of the injected light into the grating coupler. Here, a piezo-electric transducer (PZT) from Physik Instrumente is used as the moving target. The OFI FM-to-AM converted output from the photonic chip is then monitored by a Thorlabs PDA50B-EC photodetector (PD).

The LD-target distance is set to approximately 2.5 m, which corresponds to τ_{ext} ∼ 24 ns. From (4), the maximum variation $\Delta\nu$ that can be observed in the moderate feedback regime is thus approximately 30 MHz.

B. HCN Gas cell characterization

As previously mentioned, an HCN gas cell is used for comparison here. Figure 5 plots the optical spectrum of the selected gas cell line that is employed for the FM-to-AM conversion, with a typical FWHM of 19 pm. The estimated sensitivity from the HCN spectrum response is approximately

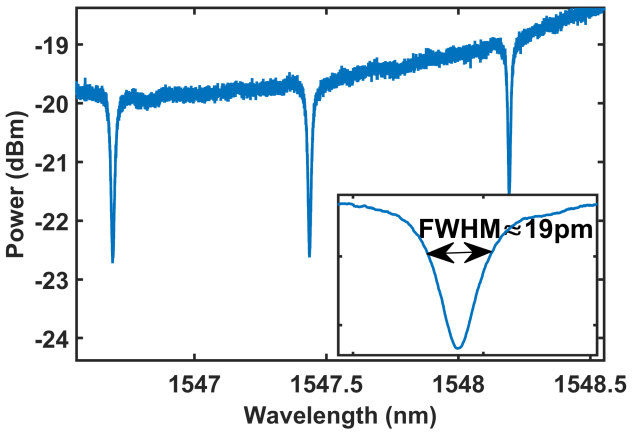

Fig. 5: Optical transmission spectrum of HCN gas cell with enlarged view of an absorption line corresponding to P branch no. 7 of gas cell.

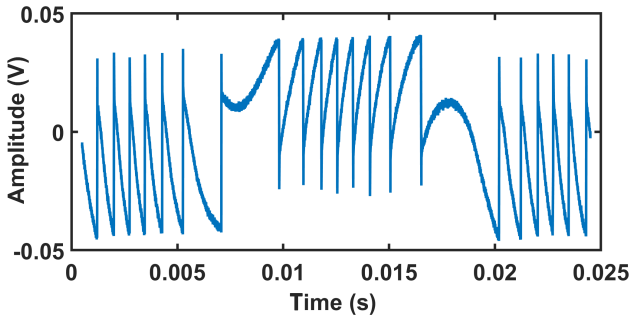

Fig. 6: Typical FM-OFI signal obtained after demodulation using HCN gas cell.

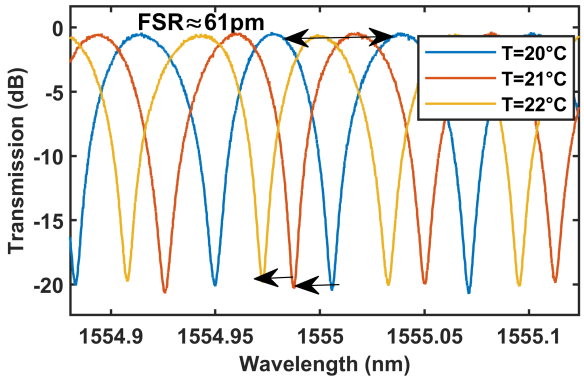

(a) $\Delta d_{path} = 2\,\text{cm}$

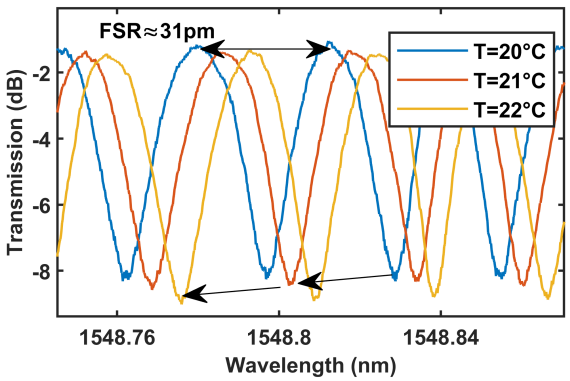

(b) $\Delta d_{path} = 4\,\text{cm}$

Fig. 7: Optical transmission spectrum of imbalanced MZI with (a) Δd_{path}= 2 cm, and (b) Δd_{path}= 4 cm. The spectra are measured with APEX206 OSA at different temperatures.

0.2 GHz^{-1} while the temperature sensitivity of this gas cell is approximately 10 fm/K. Figure 6 shows a typical FM-OFI signal demodulated by the HCN gas cell.

During experimental characterization, the PD gain is set to 10 dB. The noise equivalent displacement (NED) can then be estimated, as reported in [8], by:

$$NED = \frac{\lambda}{2}\frac{V_{RMS}}{V_{pp}}, \tag{14}$$

where V_{pp} is the peak-to-peak amplitude of one interferometric fringe of the OFI signal and V_{RMS} the OFI RMS noise, as detected by the PD. The resulting NED achieved is thus found to be approximately 5.6 nm over a 1 kHz bandwidth.

C. MZI characterization

Figures 7 (a) and (b) plot the optical transmission spectrum of the 2 cm and 4 cm imbalanced MZI, respectively, that has been captured using an APEX206 optical spectrum analyzer (OSA). Their FSR is approximately 61 pm and 31 pm respectively, measured between the peaks of two adjacent fringes (see Fig. 7 (b)). The corresponding sensitivities are subsequently esimated to be $\sim 0.37\,\text{GHz}^{-1}$ and $\sim 0.65\,\text{GHz}^{-1}$. The temperature dependence of the MZI spectral response is ∼-21 pm/K and ∼-22 pm/K for the 2 cm and 4 cm imbalanced MZI, respectively. This temperature dependence is almost 3 decades higher than for the gas cell. A temperature regulator is thus employed to reduce and control this temperature dependence. Note that the MZI spectrum (Fig. 7) also takes into account both the injection loss into the integrated photonic circuit via the grating couplers (∼ 6.5 dB/coupler), and the propagation loss (∼ 2 dB/cm) in the SiN waveguide.

D. MRR characterization

Figure 8 illustrates the optical transmission spectrum of the MRR, also measured using the APEX206 OSA. The measured FSR is approximately 1.6 nm and the FWHM is ∼12 pm (corresponding to a quality factor of 130,000), approximately similar to those of the 4- cm imbalanced MZI. From the measured FWHM, the sensitivity is estimated to be $\sim 1\,\text{GHz}^{-1}$. The temperature dependence of the MRR's spectral response is ∼21 pm/K.

E. OFI FM-to-AM noise performances

Figure 9 illustrates typical OFI signals obtained after OFI FM-to-AM conversion using the integrated 2- cm and 4- cm imbalanced MZIs, and MRR. The PD is here set to a gain

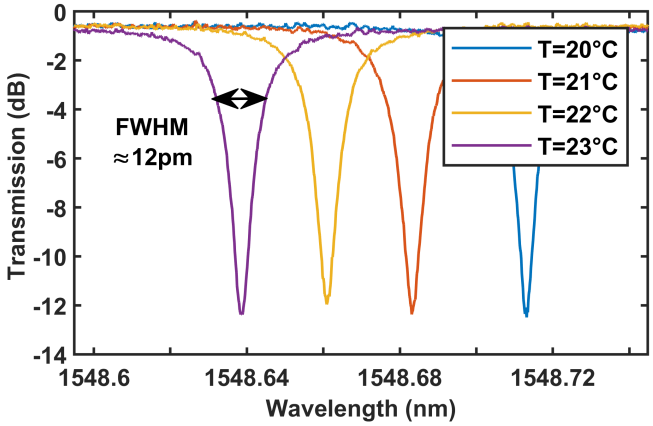

Fig. 8: Optical transmission spectrum of MRR with 120 µm radius measured with APEX206 OSA at different temperatures.

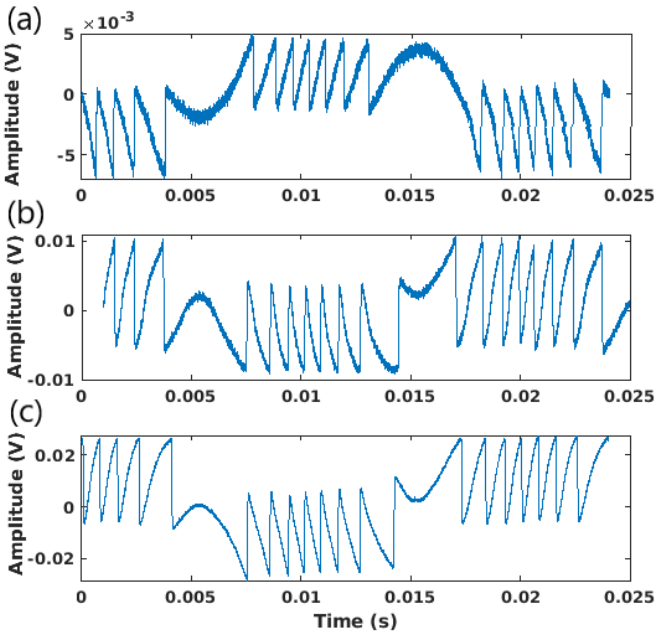

Fig. 9: OFI output signal obtained after OFI FM-to-AM conversion using: (a) 2-cm imbalanced MZI, (b) 4-cm imbalanced MZI and, (c) MRR for a PZT target vibrating at 50 Hz with 3-µm amplitude

of 40 dB. The corresponding NEDs obtained are approximately 25.4 nm, 11.5 nm and 4.9 nm for a 1 kHz bandwidth. As expected, a higher sensitivity results in better noise performances. A minor non-linearity can be observed between the estimated steep sensitivities (0.37, 0.65 and 1 GHz^{-1}, respectively) of the filters and the measured NED of OFI signals. This is likely due to the slight variation of the coupling efficiency of grating couplers associated with each structures and thermal drift of the filters. This, however, suggests that even better performances can be expected if the losses induced by both the grating couplers and in-guide propagation are reduced.

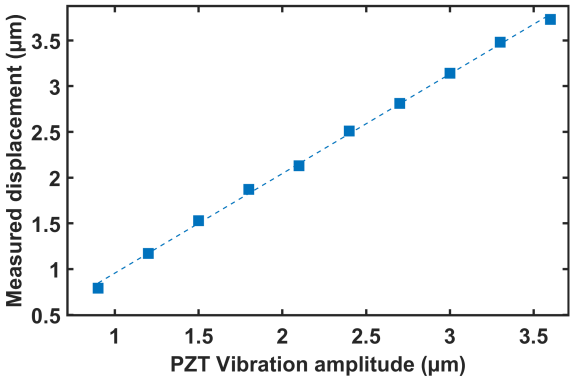

Fig. 10: NUS approach for displacement reconstruction of target vibrating at 50 Hz using the MRR to perform the FM-to-AM conversion.

F. OFI FM-to-AM displacement reconstruction

The OFI FM-to-AM signal can then be used to retrieve the target displacement using, for instance, the non-uniform sampling (NUS) approach [14]. The advantage of NUS is that it only requires the detection of the fringes contrary to other unwrapping techniques which also additionally require an additional step to unwrap the phase evolution or variation induced by displacements [17]. NUS is thus intrinsically more resilient to any drift from the optical filter's half-edge position that may induce unwanted distortion to the unwrapped signals. Figure 10 shows the NUS-based reconstructed displacement that is compared to the reference PZT.

V. Discussion

Tuning of the MZI and MRR optical signature positions could be facilitated by including either thermo-optical or electro-optical capabilities. In fact, the use of devices such as micro-heaters or electro-optical modulators can not only allow more accurate localized temperature regulation but could also simultaneously enable the application of useful dithering signals to modulate the cavity phase condition. The dithering technique has previously been proven to facilitate measurements of low or very low amplitude displacements [14].

Noise performances may be further improved by applying index-matching optical gel to improve the light injection into the chip and reduce parasitic vibrations. In this case, injection losses could also be reduced by using fiber chip engineere tapers or edge couplers instead, which requires additional processing steps such as deep-etching and/or polishing of the chip side-walls.

All the optical components used in the setup (see Fig. 2), could potentially be implemented in integrated photonics. Both the optical splitter and circulator are functions that have already been integrated on photonic chips [18]. Here, as a proof-of-concept toward this ultimate goal, an OFI sensing arm

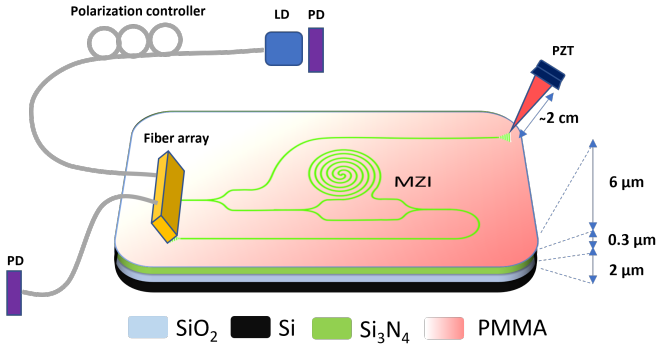

Fig. 11: Schematic diagram of OFI system integrating the OFI path with a simple Bragg grating coupler as antenna to steer the beam toward the PZT target and the FM-to-AM filter based on a 2-cm imbalanced MZI.

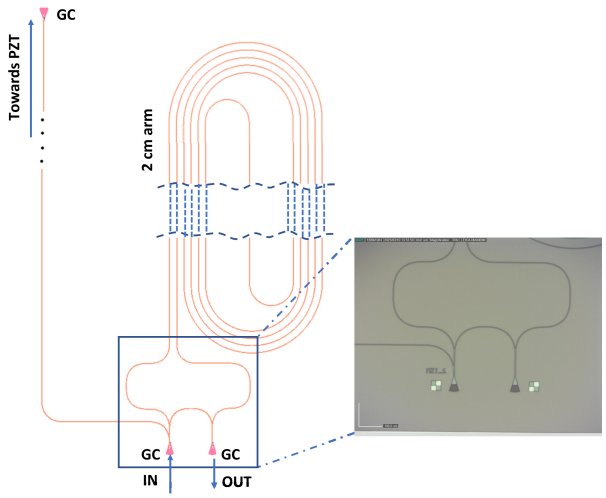

Fig. 12: Layout of OFI system integrating OFI path with simple Bragg grating coupler (GC) as antenna and a 2-cm imbalanced MZI (right: partial photo of PIC).

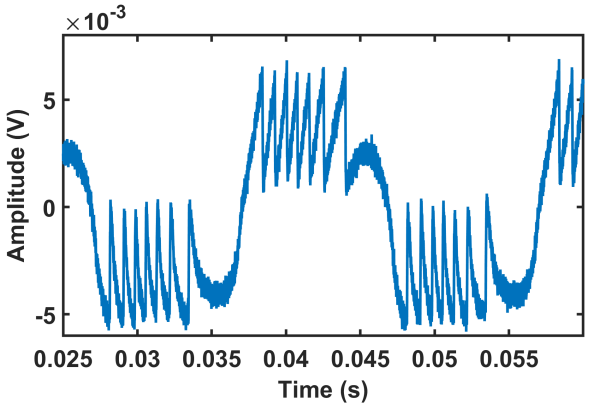

Fig. 13: OFI output signal obtained with PIC including OFI path and OFI FM-to-AM conversion using 2-cm imbalanced MZI; PZT target vibrating at 50 Hz with 3-µm amplitude

together with its FM-to-AM conversion filter based on a 2-cm MZI have been implemented (see Fig. 11). Its corresponding layout is illustrated in Fig. 12.

The grating coupler at the top end of the main strip waveguide (see Fig. 11; emitted interrogating beam pointed at PZT target) is used as a crude antenna to emit the laser beam toward the target placed at approximately 2 cm from the PIC and recover the back-scattered light. The detected signal is shown in Fig. 13 for a 3-µm displacement, thus demonstrating the feasibility of such a setup. The estimated NED for this experimental setup is approximately 50 nm, which is approximately two times larger than that obtained with the standalone 2-cm imbalanced MZI. This is potentially due to four main reasons: (1) the optical power processed by the MZI is 40% lower than in the previous system as a 50/50 Y splitter is used instead of an 80/20 coupler; (2) higher mechanical noise is induced by the setup to position the PZT next to the PIC; (3) there is no isolator or circulator to isolate the FM-to-AM converter from the main OFI path, which could result in unwanted feedback from this processing branch, and (4) backscattered light at the target goes through multiple grating couplers before reinjection into the LD, thereby additioning coupling losses.

VI. Conclusion

We have demonstrated the proof-of-concept to fully integrate an OFI FM-to-AM conversion function for OFI applications. The measured sensitivities of the 2-cm and 4-cm imbalanced MZIs are 0.37 GHz^{-1} and 0.65 GHz^{-1} respectively. For the MRR, a sensitivity of 1 GHz^{-1} has been achieved for an FWHM of 12 pm. The NEDs obtained in this work are found to be approximately 25.4 nm, 11.5 nm and 4.9 nm for the three structures, respectively. These results are more than one to two orders of magnitude larger than those reported in [8]. Nevertheless, the sensitivity could be enhanced in future design with longer imbalanced MZI and shorter LD-target distance, for instance. In addition, noise performances can also greatly benefit from better injection efficiency by exploiting edge couplers [19] instead of grating couplers, and by reducing the waveguide propagation loss down to a few dB's/m, as reported in [20]. It is also interesting to note that the performances achieved are similar to those obtained with the HCN gas cell in terms of sensitivity and NED, although the HCN gas cell is far more immune to temperature-induced drifts. Integrated heaters are currently being implemented to stabilize temperature variations on the integrated chip.

The advantages of the integrated OFI FM-to-AM conversion are its compactness, its ability to be electrically tuned as well as its facility to be thermo-regulated more efficiently compared to fiber based approaches. To achieve higher sensitivity, other types of filters based on integrated photonic filters can also be envisioned. This integrated OFI FM-to-AM conversion capability can provide an innovative pathway to integrated OFI systems applied to MEMS sensing, chemical sensing or microfluidic applications.

ACKNOWLEDGMENT

All fabrication and characterization of the integrated photonic filters were supported by both ANR-20-CE42-0010 PICSONDE in consultation with ACOEM (T. MAZOYER), and LAAS-CNRS micro and nanotechnologies platform members of the French RENATECH network (F. Carcenac, A. Lecestre and L. Mazenq).

REFERENCES

[1] S. Donati, "Developing self-mixing interferometry for instrumentation and measurements," *Laser & Photonics Reviews*, vol. 6, no. 3, pp. 393–417, 2012.

[2] T. Taimre, M. Nikolić, K. Bertling, Y. L. Lim, T. Bosch, and A. D. Rakić, "Laser feedback interferometry: a tutorial on the self-mixing effect for coherent sensing," *Adv. Opt. Photon.*, vol. 7, pp. 570–631, Sep 2015.

[3] A. Magnani, A. Pesatori, and M. Norgia, "Self-mixing vibrometer with real-time digital signal elaboration," *Appl. Opt.*, vol. 51, pp. 5318–5325, Jul 2012.

[4] N. Ali, U. Zabit, and O. D. Bernal, "Nanometric vibration sensing using spectral processing of laser self-mixing feedback phase," *IEEE Sensors Journal*, vol. 21, no. 16, pp. 17766–17774, 2021.

[5] F. P. Mezzapesa, A. Ancona, T. Sibillano, F. De Lucia, M. Dabbicco, P. M. Lugarà, and G. Scamarcio, "High-resolution monitoring of the hole depth during ultrafast laser ablation drilling by diode laser self-mixing interferometry," *Optics letters*, vol. 36, no. 6, pp. 822–824, 2011.

[6] M. Naveed and U. Zabit, "Real-time adaptive spectral filter based parasitic vibration cancellation in self-mixing laser sensor signals," *IEEE Sensors Journal*, vol. 21, no. 21, pp. 24371–24378, 2021.

[7] R. Lang and K. Kobayashi, "External optical feedback effects on semiconductor injection laser properties," *IEEE Journal of Quantum Electronics*, vol. 16, no. 3, pp. 347–355, 1980.

[8] M. Norgia, D. Melchionni, and S. Donati, "Exploiting the fm-signal in a laser-diode smi by means of a mach–zehnder filter," *IEEE Photonics Technology Letters*, vol. 29, pp. 1552–1555, Sep. 2017.

[9] V. Contreras, J. Lonnqvist, and J. Toivonen, "Edge filter enhanced self-mixing interferometry," *Opt. Lett.*, vol. 40, pp. 2814–2817, Jun 2015.

[10] M. Norgia, F. Bandi, A. Pesatori, and S. Donati, "High-sensitivity vibrometer based on fm self-mixing interferometry," in *Journal of Physics: Conference Series*, vol. 1249, p. 012020, IOP Publishing, 2019.

[11] C. Deleau, T. Apiphatnaphakul, H. C. Seat, F. Surre, U. Zabit, F. Carcenac, P.-F. Calmon, T. Bosch, and O. Bernal, "Towards integrated optical feedback fm-to-am conversion in silicon nitride for displacement sensing applications," in *2022 IEEE Sensors*, pp. 1–4, 2022.

[12] L. Tang, Y. Li, J. Li, S. Yang, H. Chen, and M. Chen, "Temperature-insensitive mach–zehnder interferometer based on a silicon nitride waveguide platform," *Opt. Lett.*, vol. 45, pp. 2780–2783, May 2020.

[13] O. D. Bernal, U. Zabit, and T. Bosch, "Classification of laser self-mixing interferometric signal under moderate feedback," *Appl. Opt.*, vol. 53, pp. 702–708, Feb 2014.

[14] O. D. Bernal, U. Zabit, F. Jayat, and T. Bosch, "Sub-λ/2 displacement sensor with nanometric precision based on optical feedback interferometry used as a non-uniform event-based sampling system," *IEEE Sensors Journal*, vol. 20, no. 10, pp. 5195–5203, 2020.

[15] A. Yariv, "Universal relations for coupling of optical power between microresonators and dielectric waveguides," *Electronics Letters*, vol. 36, pp. 321 – 322, 03 2000.

[16] L. Chrostowski and M. Hochberg, *Silicon Photonics Design: From Devices to Systems*. Cambridge University Press, 2015.

[17] C. Bes, G. Plantier, and T. Bosch, "Displacement measurements using a self-mixing laser diode under moderate feedback," *IEEE Transactions on Instrumentation and Measurement*, vol. 55, pp. 1101–1105, Aug 2006.

[18] P. Aleahmad, M. Khajavikhan, D. Christodoulides, and P. LiKamWa, "Integrated multi-port circulators for unidirectional optical information transport," *Scientific Reports*, vol. 7, p. 2129, May 2017.

[19] R. Marchetti, C. Lacava, L. Carroll, K. Gradkowski, and P. Minzioni, "Coupling strategies for silicon photonics integrated chips," *Photonics Research*, vol. 7, no. 2, pp. 201–239, 2019.

[20] J. Liu, G. Huang, R. N. Wang, J. He, A. S. Raja, T. Liu, N. J. Engelsen, and T. J. Kippenberg, "High-yield, wafer-scale fabrication of ultralow-loss, dispersion-engineered silicon nitride photonic circuits," *Nature communications*, vol. 12, no. 1, pp. 1–9, 2021.